The IFNγ-induced shift to glycolysis in microglia is associated with changes in iron handling by cells

R Holland, A McIntosh, O Finucane, V. Mela, A. Rubio-Araiz, G Timmons, S McCarthy[§]
Gun'ko YK[§] and M. A. Lynch*

Trinity College Institute for Neuroscience and [§]School of Chemistry,
Trinity College,
Dublin 2,
Ireland.

Running title: IFNγ-induced metabolic signature in microglia

Keywords: Microglial activation, IFNγ, metabolic signature, iron handling, IL-4, astrocytes

*Corresponding author
Email: lynchma@tcd.ie

ABSTRACT

Microglia, like macrophages, can adopt inflammatory and anti-inflammatory phenotypes depending on the stimulus. At the polar ends of the spectrum of phenotypes are the so-called M1-like inflammatory cells and M2-like anti-inflammatory cells that are stimulated in vitro by lipopolysaccharide (LPS) or interferon-γ (IFNγ) and interleukin-4 (IL-4) respectively. In macrophages, the evidence indicates that these phenotypes have different metabolic profiles with M1-like cells switching to glycolysis as their main source of ATP and M2-like cells utilizing oxidative phosphorylation. There is a paucity of information regarding the metabolic signatures in inflammatory and anti-inflammatory microglial phenotypes. Here, we polarized primary microglia with IFNγ and show that the characteristic increases in nitric oxide synthase 2 (NOS2) and tumor necrosis factor-α (TNFα) were accompanied by increased glycolysis and an increase in the expression of 6-phosphofructo-2-kinase/fructose-2,6-biphosphatase (PFKFB)3, an enzyme that plays a significant role in driving glycolysis. These changes were associated with increased expression of ferritin and retention of iron in microglia. In contrast with the IFNγ-induced changes IL-4, which predictably increased mRNA expression of mannose receptor C, type 1 (MRC-1) and arginase 1 (Arg1), also increased oxygen consumption in microglia. The data indicate distinct metabolic signatures of inflammatory and anti-inflammatory microglia that are also distinguishable by their iron handling profiles.

INTRODUCTION

Microglia are particularly plastic cells. They express a huge array of receptors on their cell surface and therefore they respond to numerous stimuli. Some years ago, the cells were broadly characterized into M1-like and M2-like phenotypes, paralleling the phenotypes identified in macrophages following stimulation *in vitro* with interferon-γ (IFNγ) and IL-4 respectively. It is now clear that numerous phenotypes exist *in vivo* and that the M1- and M2-like phenotypes may represent the two extremes of a spectrum of phenotypes with significant functional heterogeneity (Hu et al., 2015). The M1-like phenotype is identified by increased expression of markers such as nitric oxide synthase 2 (NOS2) and tumor necrosis factor-α (TNFα) and other inflammatory cytokines, whereas the M2-like phenotype, of which there are a number of subtypes, is associated with increased mRNA expression of mannose receptor C, type 1 (MRC-1), arginase 1 (Arg1), anti-inflammatory cytokines like IL-10 and growth factors (Hu et al., 2015). The co-existence of markers of the 2 polarized states has been reported in the same cell, for example following traumatic brain injury (Morganti et al., 2016) and following stimulation with LPS and IL-4 (Fenn et al., 2014). Furthermore gender- and age-related differences in cell polarization have been described (Crain et al., 2013) with an age-related polarization towards an inflammatory phenotype that is also evident in microglia from transgenic mice that overexpress amyloid precursor protein (APP) and presenilin 1 (PS1) (Minogue et al., 2014; Jones et al., 2015).

It is well established that macrophage activation is accompanied by metabolic reprogramming, with differentially polarized cells adopting different metabolic profiles. Specifically, M1-like macrophages are characterized by increased aerobic glycolysis and impaired oxidative metabolism (Galvan-Pena and O'Neill, 2014). This metabolic switch facilitates the rapid production of ATP necessary to support the appropriate immune functions and, because the electron transport chain is downregulated, it is also associated with increased production of reactive oxygen species (ROS) (Galvan-Pena and O'Neill, 2014). The rate-limiting step in the glycolytic pathway is the conversion of fructose-6-phosphate to fructose-1, 6-bisphosphate by phosphofructokinase (PFK1). Phosphorylation and activation of PFK1 is driven by 6-phosphofructo-2-kinase/fructose-2,6-biphosphatase

(PFKFB)3, a member of the PFKFB family of bifunctional isozymes (Pilkis et al., 1981). These enzymes contain both a phosphatase and a kinase domain and, in the case of PFKFB3, the kinase:phosphatase activity ratio of PFKFB3 is 740:1 (Sakakibara et al., 1997) contrasting with PFKFB1 in which the kinase:phosphatase activity ratio is approximately 1:1. Interestingly, PFKFB3 siRNA has been shown to attenuate iNOS and COX2 expression in M1 macrophages (Rodriguez-Prados et al., 2010). In contrast to the increase in glycolysis that is associated with M1-like macrophages, oxidative respiration and increased fatty acid oxidation characterize M2-like anti-inflammatory macrophages (Mills and O'Neill, 2016).

There has been little emphasis on the study of metabolic changes in microglia. In the microglial cell line, BV2 cells, the LPS and IFNγ-induced polarisation was shown to be accompanied by increased glucose uptake and expression of glycolytic enzymes, suggesting this phenotype is supported by enhanced glycolytic activity (Gimeno-Bayon et al., 2014). Specifically, LPS increased extracellular acidification rate (ECAR) and decreased oxygen consumption rate (OCR) (Volobouéva et al., 2013).

We set out to determine whether the polarization state induced by IFNγ in microglia was associated with a metabolic shift towards glycolysis. The data indicate that IFNγ increased ECAR and that this was associated with an increase in PFKFB3 mRNA and protein and linked with increased ferritin suggesting that IFNγ-stimulated cells sequester iron. IFNγ also induced an inflammatory phenotype in astrocytes, but there was no evidence of a shift in metabolism similar to that identified in microglia.

MATERIALS AND METHODS

Animals

C57/BL6 mice were used in these experiments; adult mice were used to prepare BMDMs and neonatal C57/BL6 mice were used to prepare cultured microglia and astrocytes. All experiments were performed under license from the Health Products Regulatory Authority of Ireland in accordance with EU regulations and with local ethical approval (Trinity College Dublin). Animals were housed under controlled conditions (20-22°C, food and water *ad lib*) and maintained under veterinary supervision.

Preparation of primary glial cultures

Microglia were prepared as previously described (Costello et al., 2015). Briefly, isolated mixed glia from cortical tissue of neonatal mice were cultured in T2 cm^2 flasks in cDMEM supplemented with macrophage colony stimulating factor (M-CSF; 100ng/ml; R&D Systems, UK) and granulocyte macrophage colony stimulating factor (GM-CSF; 100ng/mL; R&D Systems, UK) for 10-12 days, after which time non-adherent microglia were seeded in 6 well plates ($3x10^5$cells/well) and cultured for a further 2 days. To prepare astrocytes, mixed glia were cultured as above but in the absence of growth factors and after 10-12 day, cultures were shaken for 1h to remove non-adherent microglia and the remaining astrocytes were harvested following incubation for 5 min in the presence of trypsin-ethylenediaminetetraacetic acid (EDTA; 3ml per flask). Astrocytes were seeded in 6 well plates ($3x10^5$cells/well) and cultured for a further 2 days. For both microglia and astrocytes, medium was replaced with fresh cDMEM ± IFNγ (50ng/ml) or ± IL-4 (20ng/ml; both R&D Systems, UK) and incubation continued for 24h after which time cells were harvested for analysis of mRNA or western immunoblotting or for analysis of metabolic markers using Seahorse technology.

Microglia from transcardially-perfused APP/PS1 and wildtype mice were prepared as previously described (Jones et al., 2015). Briefly, tissue was cross-chopped, mechanically dissociated, passed through a 70μm filter, resuspended in 75% Percoll solution and overlaid

with 25% Percoll solution and PBS. Samples were centrifuged (800g, 10min, 4°C), the enriched microglial population was removed from the 25-75% Percoll interface, washed and centrifuged. Samples were resuspended in SeaHorse mitochondrial stress test assay media and the metabolic profile was assessed as described below.

Preparation of BMDM

BMDMs were isolated from the marrow of the femurs and tibias of mice as described (Barrett et al., 2015). Briefly, the marrow was flushed into a sterile falcon tube in Dulbecco's modified Eagle's medium (DMEM; 500ml; Invitrogen, UK) supplemented with heat-inactivated foetal bovine serum (FBS; 50ml; 10%; Gibco, UK) and penicillin-streptomycin (5ml; 1%; Gibco, UK), the cell suspension was triturated, filtered into a sterile tube and centrifuged (400 x g, 5 minutes) to yield a pellet that was resuspended in red blood cell lysis buffer (Sigma Aldrich, UK) for 1 min. The addition of DMEM terminated the lysis, the suspension was centrifuged (400 x g, 5 minutes) and the cells were washed, centrifuged (400 x g, 5 minutes) and resuspended in DMEM supplemented with L929 conditioned media (20%). Cells were seeded in sterile cell culture T75cm^2 flasks, non-adherent cells were removed on day 2, media was replaced, and cells were cultured for a further 6 days, with the media replaced on day 4. On day 6, cells were transferred to 6-well plates (0.5 x 10^6 cells per well) and cultured for a further 2 days, incubated in the presence/absence of IFNγ or IL-4 and harvested as described above.

Analysis of mRNA expression by real-time PCR

RNA was isolated from cells using a Nucleospin® RNAII kit (Macherey-Nagel GmbH, Germany) and reverse transcribed into cDNA using a High-Capacity cDNA Archive kit (Applied Biosystems, UK) as per manufacturer's instructions. Assay ID's for the genes examined were: β-actin (Mm00407939_s1), TNFα (Mm00443258_m1), NOS2 (Mm0040502_m1), MRC1 (Mm00485148_m1), Arg1 (Mm00475988_m1), CD40 (Mm00441891_m1), IL-1β (Mm00434228_m1) IGF1 (Mm00439560_m1), ferritin (Mm00850707_g1), ferroportin (Mm01254822_m1), PFKFB1 (Mm01256237_m1) and PFKFB3 (Mm00504650_m1). Real-time PCR was performed using an ABI Prism 7300 instrument (Applied Biosystems, UK) with β-actin used as the endogenous control. In all cases, relative gene expression was calculated with reference to untreated BMDMs using the ΔΔCT method with Applied Biosystems RQ software (Applied Biosystems, UK).

Western immunoblotting

Microglia were prepared for western immunoblotting as described (Dempsey et al., 2016). Briefly, cells were incubated in lysis buffer (composition in mM: Tris-HCl 10, NaCl 50, $Na_4P_2O_7.H_2O$ 10, NaF 50, containing 1% each of Igepal, phosphatase inhibitor cocktail I and II, and protease inhibitor; Sigma, UK), equalized for protein, added to 4x SDS sample buffer (composition: Tris-HCl 100mM, pH 6.8, 4% SDS, 2% bromophenol blue, 20% glycerol; Sigma, UK), boiled (100°C, 5 min) and applied to 10% SDS gels. Proteins were transferred to nitrocellulose membrane, non-specific binding was blocked and membranes were incubated overnight at 4°C with the antibodies raised against ferritin, ferroportin (SLA-40A1), PFKFB1 or PFKFB3 (all IgG, raised in rabbit, 1:1000 in 5% non-fat dried milk/TBS-T; AbCam, US). Membranes were washed and incubated (room temperature, 2h) with a secondary HRP-linked anti-rabbit antibody (1:5000 in 5% milk in TBS-T). Immunoreactive bands were detected using WesternBright ECL chemiluminescent substrate (Advansta, US). Images were captured using the Fujifilm LAS-4000 imager and densitometric analysis was carried out using ImageJ (http://rsb.info.nih.gov/).

ELISA

The concentrations of CCL2, CCL3 and CCL5 were assessed in supernatant samples from cultured microglia as previously described (Minogue et al., 2012), using mouse DuoSet ELISA kits (CCL2/MCP1, CCL3/MIP1α, CCL5/RANTES R&D Systems, US). Briefly, 96-well plates (Nunc-Immuno plate with Maxisorp surface, Denmark) were coated with capture antibody (100µl/well) and incubated (overnight, room temperature). Duplicate samples or standards (50µl/well) were added and plates were incubated (24h, 4ºC) and washed before addition of detection (biotinylated goat anti-mouse) antibody for (1h, room temperature). Plates were washed, incubated with streptavidin-horseradish peroxidase conjugate (20 min, room temperature) and washed before addition of substrate solution (50µl; 1:1 H_2O_2:tetramethylbenzidine; R&D Systems, US). After colour development, the reaction was stopped by adding 1M H_2SO_4 (25µl) and plates were read at 450nm (Labsystem Multiskan RC, UK).

Metabolic analysis

The SeaHorse Extracellular Flux (XF24) Analyser (SeaHorse Bioscience, US) was used to carry out bioenergetic analysis of cells. Microglia ($1x10^5$cells/well), astrocytes ($8x10^4$cells/well) and BMDMs ($2x10^5$cells/well) were seeded (100µl/well) in SeaHorse cell culture microplates and incubated at room temperature for 1h and subsequently at 37°C for 1h. cDMEM (150µl) was added to each well, cells were incubated (24h, 37°C, humidified 5% CO2; 95% air) and incubated in cDMEM ± IFNγ (50ng/ml) or ± IL-4 (20ng/ml). The sensor cartridge was hydrated by adding SeaHorse XF Calibrant solution (1ml; SeaHorse BioScience, US) to each well of the utility plate and samples were left overnight in a CO_2-free incubator at 37°C. Following incubation, cells were washed twice with the assay medium for the mitochondrial stress test or the glycolytic flux test (1ml) according to the manufacturer's instructions, specific assay media was added to give a final volume of 475µl/well and the plate was incubated in a CO_2-free incubator at 37°C for 1h. For the mitochondrial stress test, oligomycin (20µM; Abcam, UK), carbonyl cyanide-4-(trifluoromethoxy)phenylhydrazone (20µM; FCCP; Sigma-Aldrich, UK) and antimycin A (40µM; Sigma-Aldrich, UK) were loaded into the appropriate ports for sequential delivery. For the glycolytic flux test, glucose (10mM), oligomycin (20µM) and 2-deoxy-D-glucose (2-DG; 500mM; all Sigma-Aldrich, UK) were prepared in glycolytic flux assay media and similarly loaded into the appropriate ports. Following calibration, oxygen consumption rate (OCR) and extracellular acidification rate (ECAR) were measured every 8 min for 96 min and the appropriate compounds were injected sequentially at 24 min intervals. ECAR and OCR were automatically calculated using the SeaHorse XF24 software and 4-6 replicates were assessed for each separate sample.

Uptake of fluorescently-labelled iron particles

Microglia were plated onto coverslips coated with poly-D-lysine (5 µg/ml; Merck Millipore Ltd, UK), acclimatised for 48h and incubated with IFNγ (50ng/ml) for 24h. Cells were washed and incubated with serum free media ± iron oxide nanoparticles (IONP) fluorescently tagged with ATTO (100µg/ml; 7-10nm in diameter) for 2h. Coverslips were washed in PBS, fixed in 4% PFA (30 min) and stored in PBS at 4°C for later analysis. Cells were permeablized with PBS-T and blocked for 1h (10% NHS and 0.1% Triton X-100) before incubation with primary anti-Iba1 (Wako, Japan 1:1000) and secondary Alexa Fluor® 594 donkey anti-rabbit IgG (1:1000) antibodies. Coverslips were mounted in ProLong®Gold with the nuclear marker DAPI (Thermo Scientific, US). Z-stack images (10 slices; 5 fields of view; 60X magnification; duplicate analysis) were acquired using the Leica SP8 scanning confocal microscope and a single slice with no

membrane-bound IONP was selected for analysis. IONP fluorescence intensity was analysed using ImageJ software and the corrected total cellular fluorescence (TCCF) per $Iba1^+$ cell was calculated by TCCF = integrated density – (area of selected cell × mean fluorescence of background readings) (McCloy et al., 2014).

Statistical analysis

Data are presented as the mean ± SEM. Statistical analysis was carried out using an unpaired Student's *t*-test or a 1-way ANOVA with Dunnett's post-hoc tests as indicated in figure legends.

RESULTS

Incubation of BMDMs with IFNγ resulted in the predicted increase in mRNA expression of TNFα and iNOS (**p < 0.01; ***p < 0.001; student's t-test for independent means; Figure 1A,B). Cells were assessed for evidence of a change in metabolic profile by evaluating ECAR and OCR and the data indicate that IFNγ significantly increased glycolysis and glycolytic capacity (*p < 0.05; Figure 1C-E). Analysis of the effect of IFNγ on OCR revealed that it exerted no significant effect on basal respiration (Figure 1F,G) while maximal respiration was increased (*p < 0.05; Figure 1H). PFKFB3 is a key driver of glycolysis because of its ability to stimulate phosphofructokinase 1 and we show that PFKFB3 mRNA was significantly increased in IFNγ-stimulated BMDMs whereas PFKFB1 was significantly decreased (*p < 0.05; Figure 1I,J); the ratio PFKFB3:PFKFB1 was also significantly increased (*p < 0.05; Figure 1K). These changes were accompanied by a decrease in expression of the iron transport protein, ferroportin, but no change in expression of ferritin mRNA (*p < 0.05; Figure 1L,M).

We then assessed the effect of IFNγ on microglia and show that it triggered a significant increase in TNFα and iNOS and also in CD40mRNA and IL-1β mRNA (*p < 0.05; **p < 0.01; ***p < 0.001; Figure 2A-D) and an increase in release of the chemokines CCL2, CCL3 and CCL5 (**p < 0.01; ***p < 0.001; Figure 2E-G). IFNγ decreased mRNA expression of MRC1, Arg1 and IGF-1, which are markers of the M2-like phenotype (***p < 0.001; Figure 2H-J). We investigated the effect of IFNγ on metabolic changes in microglia and show that it stimulated glycolysis in microglia, as it did in BMDM (**p < 0.01; student's t-test for independent means; Figure 3A,B), but did not affect glycolytic capacity or glycolytic reserve (Figure 3C,D). Again, the data indicate that the increase in glycolysis was associated with increases in PFKFB3 mRNA and the ratio PFKFB3:PFKFB1, whereas PFKFB1 mRNA was decreased (*p < 0.05; **p < 0.01; Figure 3E-G). Analysis of PFKFB3 by western immunoblotting indicated that there were 2 forms of the enzyme, the inducible form (PFKFB3(1)) and the constituitively-expressed form (PFKFB3(2)); whereas IFNγ significantly increased PFKFB3(1) (*p < 0.05; Figure 3H,J), the IFNγ-induced increase in PFKFB3(2) was not statistically significant (Figure 3I,J). Reflecting the change in mRNA expression, the ratio PFKFB3:PFKFB1 was significant increased in IFNγ-incubated microglia (***p < 0.001; Figure 3K). PFKFB1 was similar in control-incubated and IFNγ-incubated microglia (Figure 3L,M).

IFNγ significantly increased ferritin mRNA and significantly decreased ferroportin mRNA (*p < 0.05**p < 0.01; Figure 4A,B) and analysis by western immunoblotting indicated that ferritin was increased (**p < 0.01; Figure 4C) while there was no significant IFNγ-induced change in ferroportin (Figure 4D). Increased expression of ferritin probably indicates intracellular sequestration of iron and to assess this directly we examined uptake of fluorescently-labelled iron oxide particles; the data show that particle accumulation was greater in IFNγ-stimulated cells (compare panels (iii; control-treated microglia) and (iv;

IFNγ-treated microglia); Figure 4E) and that the number of $Iba1^+$ iron $oxide^+$ microglia was significantly greater following incubation with IFNγ (*$p < 0.05$; Figure 4F).

To determine the effect of IFNγ on oxidative phosphorylation, we assessed OCR and the data indicate that OCR was similar in control-treated and IFNγ-treated microglia (Figure 5A) and that basal respiration, maximal respiration and ATP production were not affected by IFNγ (Figure 5B-D).

Predictably IL-4 increased mRNA expression of MRC1 and Arg1 in microglia while it decreased TNFα and iNOS (*$p < 0.05$; ***$p < 0.001$; Figure 6A-D). These changes were associated with a significant increase in OCR and specifically in basal respiration and ATP production (**$p < 0.01$; Figure 6E-H). There was no IL-4-induced change in ECAR, glycolysis, glycolytic capacity or glycolytic reserve (Figure 6I-L). In addition, incubation of microglia in the presence of IL-4 did not change mRNA expression of PFKFB3 or PFKFB1 (Figure 6M,N) and also exerted no effect on ferritin mRNA or ferroportin mRNA (Figure 6O,P).

We assessed the effect of IFNγ and IL-4 on astrocytes and the evidence indicates that IFNγ increased TNFα and iNOS mRNA and IL-4 increased MRC1 and Arg1 mRNA (***$p < 0.001$; Figure 7A-D). IFNγ had no effect on ECAR (Figure 7E) or on glycolysis, glycolytic capacity or glycolytic reserve (Figure 7F-G), contrasting with the effect in microglia. While IL-4 induces expression of markers of the M2-like phenotype in astrocytes as it does in microglia, there is no accompanying change in metabolism (Figure 7G,H), and this also contrast with the IL-4-induced effect on OCR in microglia. Therefore while IFNγ and IL-4 induce changes reflective of M1-like and M2-like phenotypes in both microglia and astrocytes, accompanying change in metabolism are confined to microglia.

DISCUSSION

We set out to determine whether changes in metabolism in microglia accompanied the changes in phenotypic markers induced by IFNγ and IL-4. The significant finding is that IFNγ, which predictably increased mRNA expression of TNFα and iNOS, triggered an increase in glycolysis and expression of PFKFB3 and increased iron retention reflected by an increase in ferritin and increased engulfment of iron oxide particles. While IFNγ increased expression of markers that are reflective of the M1-like phenotype in astrocytes, there was no indication of a metabolic switch to glycolysis.

In the past few years an inextricable link between metabolism and immune cell function has been identified (Rodriguez-Prados et al., 2010; Michalek et al., 2011; Pearce and Everts, 2015; Mills and O'Neill, 2016). Here we show that the anticipated IFNγ-induced increase in TNFα and iNOS in BMDMs was accompanied by evidence of increased glycolysis This observation in macrophages is consistent with other studies that have reported increases in ECAR in BMDMs stimulated with LPS (Haschemi et al., 2012) or LPS and IFNγ (Huang et al., 2014), although the present data indicate that IFNγ alone is sufficient to drive this change.

Of particular significance, is the finding that the IFNγ-induced increase in glycolysis observed in BMDMs, was paralleled in microglia. The IFNγ-driven metabolic shift was accompanied by increased expression of markers of the M1-like phenotype, TNFα, iNOS, IL-1β and CD40, increased release of CCL2, CCL3 and CCL5, and decreased expression of MRC1 and IGF-1, which are markers of M2-like cells. The metabolic signatures of differentially activated microglia has not been studied to any significant extent, although it has been shown that LPS decreases OCR and increases ECAR (Orihuela et al., 2016) and that LPS+IFNγ stimulates lactate release and other hallmarks of glycolysis (Gimeno-Bayon et al., 2014) in BV2 cells. At least in dendritic cells, one significant factor that drives the

shift to glycolysis is NO, produced as a result of iNOS upregulation, which inhibits mitochondrial metabolism (Everts et al., 2012).

The metabolic switch to glycolysis that can occur in the presence of oxygen, aerobic glycolysis, is described as the Warburg effect (Palsson-McDermott and O'Neill, 2013). It is a characteristic of proliferating cells and mediated by PFKFB3 (Yalcin et al., 2014). In an effort to determine the factors that might drive the increase in glycolysis in IFNγ-treated cells, we evaluated mRNA expression of PFKFB3 and show that it was increased in IFNγ-incubated BMDMs and microglia, and accompanied by a decrease in expression of PFKFB1. The PFKFB3:PFKFB1 ratio was also increased. These bifunctional isozymes are central to facilitating glycolysis since the kinase domain, particularly of PFKFB3, increases PFK1 activity, which converts fructose-6-phosphate to fructose-1, 6-bisphosphate. The specific role of PFKFB3 is because of a mutation in a phosphatase active site that results in a kinase:phosphatase activity ratio of approximately 740:1 (Sakakibara et al., 1997). The present findings, which demonstrate parallel increases in glycolysis and PFKFB3 expression in IFNγ-induced BMDMs, are consistent with reports of similar changes induced by LPS (Ruiz-Garcia et al., 2011; Tawakol et al., 2015). Indeed PFKFB3 is a key factor in the LPS-induced switch to glycolysis in macrophages and/or dendritic cells although others have also been identified including hypoxia-inducible factor-1α (Kelly and O'Neill, 2015). The evidence presented here is consistent with the idea that PFKFB3 plays an important in IFNγ-induced glycolysis in microglia.

The switch to glycolysis triggered by IFNγ in BMDMs was associated with a decrease in expression of ferroportin while ferritin expression was unchanged. An increase in ferritin in M1-like macrophages, which may be indicative of iron retention by cells, has been reported (Corna et al., 2010) and this contrasts with the lack of change in IFNγ-treated BMDMs reported here. However the focus in this study is on microglia and we demonstrate that ferritin mRNA and protein were both increased in IFNγ-treated M1-like microglia while ferroportin mRNA was decreased. In contrast to the effect of IFNγ on ECAR in microglia, it did not affect OCR, and basal respiration, maximal respiration and ATP production were also unaffected by IFNγ.

We examined the changes in metabolism that accompanied the markers of M2-like activation in IL-4-stimulated microglia. Significantly, IL-4 increased oxidative respiration and, although there are no previous reports of such a change in microglia, the evidence indicates that there is an increase in oxidative metabolism in IL-4-polarized M2-like macrophages (Nomura et al., 2016), a finding that we also observed (data not shown). IL-4 did not affect glycolysis in microglia and, consistent with our earlier data, had no effect on PFKFB3 mRNA.

Interestingly, astrocytes were polarized to M1-like and M2-like cells in response to IFNγ and IL-4 in a manner that was similar to the response of microglia and this is consistent with previous findings (Jang et al. 2013). However we found no evidence that polarized astrocytes adopted the metabolic signatures that were adopted by polarized microglia indicating cell-specific effects.

Identification of microglial phenotypes by assessing mRNA expression of well-defined molecules is useful for categorizing cells as inflammatory or anti-inflammatory.

The data presented here identifies a metabolic model that provides a more complete phenotypic description and, significantly, that demonstrates a shift in metabolism of microglia to glycolysis following activation with the M1 polarizing stimulus, IFNγ. The data open up the possibility that modulating metabolic pathways may significantly impact on neuroinflammatory changes.

ACKNOWLEDGEMENTS: The authors acknowledge funding from Science Foundation Ireland (11/PI/1014)

REFERENCES

Barrett JP, Minogue AM, Jones RS, Ribeiro C, Kelly RJ, Lynch MA (2015) Bone marrow-derived macrophages from AbetaPP/PS1 mice are sensitized to the effects of inflammatory stimuli. J Alzheimers Dis 44:949-962.

Corna G, Campana L, Pignatti E, Castiglioni A, Tagliafico E, Bosurgi L, Campanella A, Brunelli S, Manfredi AA, Apostoli P, Silvestri L, Camaschella C, Rovere-Querini P (2010) Polarization dictates iron handling by inflammatory and alternatively activated macrophages. Haematologica 95:1814-1822.

Costello DA, Carney DG, Lynch MA (2015) alpha-TLR2 antibody attenuates the Abeta-mediated inflammatory response in microglia through enhanced expression of SIGIRR. Brain Behav Immun 46:70-79.

Crain JM, Nikodemova M, Watters JJ (2013) Microglia express distinct M1 and M2 phenotypic markers in the postnatal and adult central nervous system in male and female mice. J Neurosci Res 91:1143-1151.

Dempsey C, Rubio Araiz A, Bryson KJ, Finucane O, Larkin C, Mills EL, Robertson AA, Cooper MA, O'Neill LA, Lynch MA (2016) Inhibiting the NLRP3 inflammasome with MCC950 promotes non-phlogistic clearance of amyloid-beta and cognitive function in APP/PS1 mice. Brain Behav Immun.

Everts B, Amiel E, van der Windt GJ, Freitas TC, Chott R, Yarasheski KE, Pearce EL, Pearce EJ (2012) Commitment to glycolysis sustains survival of NO-producing inflammatory dendritic cells. Blood 120:1422-1431.

Fenn AM, Hall JC, Gensel JC, Popovich PG, Godbout JP (2014) IL-4 signaling drives a unique arginase+/IL-1beta+ microglia phenotype and recruits macrophages to the inflammatory CNS: consequences of age-related deficits in IL-4Ralpha after traumatic spinal cord injury. J Neurosci 34:8904-8917.

Galvan-Pena S, O'Neill LA (2014) Metabolic reprograming in macrophage polarization. Frontiers in immunology 5:420.

Gimeno-Bayon J, Lopez-Lopez A, Rodriguez MJ, Mahy N (2014) Glucose pathways adaptation supports acquisition of activated microglia phenotype. J Neurosci Res 92:723-731.

Haschemi A, Kosma P, Gille L, Evans CR, Burant CF, Starkl P, Knapp B, Haas R, Schmid JA, Jandl C, Amir S, Lubec G, Park J, Esterbauer H, Bilban M, Brizuela L, Pospisilik JA, Otterbein LE, Wagner O (2012) The sedoheptulose kinase CARKL directs macrophage polarization through control of glucose metabolism. Cell metabolism 15:813-826.

Hu X, Leak RK, Shi Y, Suenaga J, Gao Y, Zheng P, Chen J (2015) Microglial and macrophage polarization-new prospects for brain repair. Nat Rev Neurol 11:56-64.

Huang SC, Everts B, Ivanova Y, O'Sullivan D, Nascimento M, Smith AM, Beatty W, Love-Gregory L, Lam WY, O'Neill CM, Yan C, Du H, Abumrad NA, Urban JF, Jr., Artyomov MN, Pearce EL, Pearce EJ (2014) Cell-intrinsic lysosomal lipolysis is essential for alternative activation of macrophages. Nat Immunol 15:846-855.

Jones RS, Minogue AM, Fitzpatrick O, Lynch MA (2015) Inhibition of JAK2 attenuates the increase in inflammatory markers in microglia from APP/PS1 mice. Neurobiol Aging 36:2716-2724.

Kelly B, O'Neill LA (2015) Metabolic reprogramming in macrophages and dendritic cells in innate immunity. Cell research 25:771-784.

McCloy RA, Rogers S, Caldon CE, Lorca T, Castro A, Burgess A (2014) Partial inhibition of Cdk1 in G 2 phase overrides the SAC and decouples mitotic events. Cell Cycle 13:1400-1412.
Michalek RD, Gerriets VA, Jacobs SR, Macintyre AN, MacIver NJ, Mason EF, Sullivan SA, Nichols AG, Rathmell JC (2011) Cutting edge: distinct glycolytic and lipid oxidative metabolic programs are essential for effector and regulatory CD4+ T cell subsets. J Immunol 186:3299-3303.
Mills EL, O'Neill LA (2016) Reprogramming mitochondrial metabolism in macrophages as an anti-inflammatory signal. Eur J Immunol 46:13-21.
Minogue AM, Barrett JP, Lynch MA (2012) LPS-induced release of IL-6 from glia modulates production of IL-1 beta in a JAK2-dependent manner. J Neuroinflammation 9:126.
Minogue AM, Jones RS, Kelly RJ, McDonald CL, Connor TJ, Lynch MA (2014) Age-associated dysregulation of microglial activation is coupled with enhanced blood-brain barrier permeability and pathology in APP/PS1 mice. Neurobiol Aging 35:1442-1452.
Morganti JM, Riparip LK, Rosi S (2016) Call Off the Dog(ma): M1/M2 Polarization Is Concurrent following Traumatic Brain Injury. PLoS One 11:e0148001.
Nomura M, Liu J, Rovira, II, Gonzalez-Hurtado E, Lee J, Wolfgang MJ, Finkel T (2016) Fatty acid oxidation in macrophage polarization. Nat Immunol 17:216-217.
Orihuela R, McPherson CA, Harry GJ (2016) Microglial M1/M2 polarization and metabolic states. Br J Pharmacol 173:649-665.
Palsson-McDermott EM, O'Neill LA (2013) The Warburg effect then and now: from cancer to inflammatory diseases. BioEssays : news and reviews in molecular, cellular and developmental biology 35:965-973.
Pearce EJ, Everts B (2015) Dendritic cell metabolism. Nat Rev Immunol 15:18-29.
Pilkis SJ, El-Maghrabi MR, McGrane MM, Pilkis J, Claus TH (1981) The role of fructose 2,6-bisphosphate in regulation of fructose-1,6-bisphosphatase. J Biol Chem 256:11489-11495.
Rodriguez-Prados JC, Traves PG, Cuenca J, Rico D, Aragones J, Martin-Sanz P, Cascante M, Bosca L (2010) Substrate fate in activated macrophages: a comparison between innate, classic, and alternative activation. J Immunol 185:605-614.
Ruiz-Garcia A, Monsalve E, Novellasdemunt L, Navarro-Sabate A, Manzano A, Rivero S, Castrillo A, Casado M, Laborda J, Bartrons R, Diaz-Guerra MJ (2011) Cooperation of adenosine with macrophage Toll-4 receptor agonists leads to increased glycolytic flux through the enhanced expression of PFKFB3 gene. J Biol Chem 286:19247-19258.
Sakakibara R, Kato M, Okamura N, Nakagawa T, Komada Y, Tominaga N, Shimojo M, Fukasawa M (1997) Characterization of a human placental fructose-6-phosphate, 2-kinase/fructose-2,6-bisphosphatase. Journal of biochemistry 122:122-128.
Tawakol A, Singh P, Mojena M, Pimentel-Santillana M, Emami H, MacNabb M, Rudd JH, Narula J, Enriquez JA, Traves PG, Fernandez-Velasco M, Bartrons R, Martin-Sanz P, Fayad ZA, Tejedor A, Bosca L (2015) HIF-1alpha and PFKFB3 Mediate a Tight Relationship Between Proinflammatory Activation and Anerobic Metabolism in Atherosclerotic Macrophages. Arterioscler Thromb Vasc Biol 35:1463-1471.
Voloboueva LA, Emery JF, Sun X, Giffard RG (2013) Inflammatory response of microglial BV-2 cells includes a glycolytic shift and is modulated by mitochondrial glucose-regulated protein 75/mortalin. FEBS Lett 587:756-762.
Yalcin A, Clem BF, Imbert-Fernandez Y, Ozcan SC, Peker S, O'Neal J, Klarer AC, Clem AL, Telang S, Chesney J (2014) 6-Phosphofructo-2-kinase (PFKFB3) promotes cell cycle progression and suppresses apoptosis via Cdk1-mediated phosphorylation of p27. Cell Death Dis 5:e1337.

FIGURE LEGENDS

Figure 1. The inflammatory changes induced by IFNγ in BMDMs are associated with a shift to glycolysis.

BMDMs, isolated from the femurs and tibias of mice were cultured for 8 days as described in the Methods and incubated with/without IFNγ (50ng/ml) for 24h. Cells were harvested for metabolic analysis using the SeaHorse Extracellular Flux (XF24) Analyser or for analysis by PCR.

IFNγ increased TNFα and iNOS mRNA (**p < 0.01; ***p < 0.001; student's t-test for independent means; Figure 1A,B) and extracellular acidification rate (C), glycolysis (D) and glycolytic capacity (E; *p < 0.05). Analysis of oxygen consumption rate (OCR) indicated that IFNγ had no significant effect on basal respiration (F,G) but increased maximum respiration (H; *p < 0.05; n=6). IFNγ also increased PFKFB3 mRNA (I) and the PFKFB3:PFKFB1 ratio (K), while it decreased PFKFB1 mRNA (J) and ferroportin mRNA (M; *p < 0.05; n=4). Data are presented as means ± SEM.

Figure 2. IFNγ increases markers of activation in microglia.

Primary microglia, prepared from neonatal mice were cultured as described in the Methods and incubated with/without IFNγ (50ng/ml) for 24h. Cells and supernatants collected for analysis by PCR or ELISA.

A-D. IFNγ significantly increased mRNA expression of TNFα, iNOS, IL-1β and CD40 (*p < 0.05; **p < 0.01; ***p < 0.001; student's t-test for independent means; n=4). E-J. IFNγ also significantly increased supernatant concentrations of CCL2 (E), CCL3 (F) and CCL5 (G; **p < 0.01; ***p < 0.001; n=8), while it decreased mRNA expression of MRC1 (H), Arg1 (I) and IGF-1 (J; ***p < 0.001; Figure 2H-J; n=8). Data are presented as means ± SEM.

Figure 3. IFNγ induces an increased in PFKFB3 and a switch to glycolysis in microglia.

Primary microglial cells ($1x10^5$cells/well) were seeded in a Seahorse XF plate (see Methods), incubated at room temperature for 1h and 37°C for 1h prior to the addition of IFNγ (50ng/ml) and overnight incubation in a CO_2-free incubator at 37°C (Seahorse Bioscience, Supporting Information).

A-D. To assess ECAR, 3 baseline measures were taken and the cells were sequentially exposed to glucose (10mM), oligomycin (20μM) and 2-deoxy-D-glucose (2-DG; 500mM); the resultant bioenergetic profile is presented (A). IFNγ significantly increased glycolysis (B; **p < 0.01; student's t-test for independent means; n=6) but not glycolytic capacity (C) or glycolytic reserve (D).

E-M. IFNγ significantly increased PFKFB3 mRNA (E) and decreased PFKFB1 mRNA (F) and this was reflected in a significant increase in the ratio PFKFB3:PFKFB1 (G; *p < 0.05; **p < 0.01; n=12). Cell lysates were assessed by western immunoblotting; IFNγ increased the inducible form, PFKFB3(1) but not the constituitively-expressed PFKFB3(2) as shown by the mean densitometric data and the representative blot (H-J; *p < 0.05; n=6), and IFNγ also increased the ratio PFKFB3:PFKFB1 (K; ***p < 0.001). No change in PFKFB1 was observed as indicated by the sample immunoblot and the mean densitometric data *L,M). Data are means ± SEM.

Figure 4. IFNγ alters iron handling by microglia.

Primary microglia, cultured from neonatal mice were cultured as described in the Methods, incubated ± IFNγ (50ng/ml) for 24h and the cells were harvested for analysis by PCR or

western immunoblotting as described in the Methods. Separately cells were plated on coverslips, incubated with IFNγ (50ng/ml) for 24h and in serum free media ± iron oxide nanoparticles (IONP) fluorescently tagged with ATTO (100μg/ml; 7-10nm in diameter) for 2h. Cells were fixed and visualized for iron oxide nanoparticle uptake (see Methods).
A-D. IFNγ significantly increased ferritin mRNA (A) and protein (C; *$p < 0.05$; **$p < 0.01$; student's t-test for independent means; n=6) and significantly decreased ferroportin mRNA (B; **$p < 0.01$) but did not affect ferroportin protein (D). Sample immunoblots for ferritin and ferroportin are shown.
E,F. Sample images are shown for control- and IFNγ-treated microglia that were incubated ± iron oxide particles (IOP) and these show that IFNγ increased the number of Iba^+ (red) IOP^+ cells. Mean values indicated that the IFNγ-induced increase was statistically significant (F; *$p < 0.05$; n=3). Data are means ± SEM.

Figure 5. IFNγ does not affect oxygen consumption in microglia.
Microglia were prepared for analysis as described in the legend to Figure 3. Three baseline measures were taken and cells were then exposed sequentially to oligomycin (20μM), carbonyl cyanide-4-(trifluoromethoxy)phenylhydrazone (20μM; FCCP) and antimycin A (40μM).
A-D. The mean data shown in the OCR bioenergetics profile indicates a minimal effect of IFNγ (A) and there was no significant effect of IFNγ on basal respiration (B), maximal respiration (C) or ATP production (D). Data are means ± SEM (n=6).

Figure 6. IL-4 increases oxygen consumption in microglia.
Primary microglia, prepared from neonatal mice, were cultured as described in the Methods and incubated ± IL-4 (20ng/ml) for 24h. Cells were harvested for metabolic analysis or for analysis by PCR.
A-D. IL-4 significantly increased MRC1 mRNA (A) and Arg1 mRNA (B) and decreased TNFα mRNA (C) and iNOS mRNA (D; *$p < 0.05$; ***$p < 0.001$; n=5).
E-L. IL-4 increased OCR as indicated by the metabolic profile (E) and significantly increased basal respiration (F) and ATP production (H; **$p < 0.01$) but not maximum respiration (G; n=10). IL-4 did not affect ECAR (I) and had no significant effect on glycolysis (J), glycolytic capacity (K) or glycolytic reserve (L; n=10).
M-P. IFNγ did not affect mRNA expression of PFKFB3 (M), PFKFB1 (N), ferritin (O) or ferroportin (P; n=8).

Figure 7. IFNγ polarizes astrocytes but does not affect metabolism.
Primary astrocytes, prepared from neonatal mice, were cultured as described in the Methods, seeded in 6 well plates ($3x10^5$cells/well) and incubated ± IFNγ (50ng/ml) or ± IL-4 (20ng/ml) for 24h.
A-D. IFNγ significantly increased mRNA expression of TNFα (A) and iNOS (B) and decreased MRC1 (C) and Arg1 (D) while IL-4 increased mRNA expression of MRC1 and Arg1 (***$p < 0.001$; 1 way ANOVA with post hoc analysis (Dunnett's test); n=7). E-F. Neither IFNγ nor IL-4 significantly affected ECAR as indicated by the metabolic profile (E) and by analysis of mean values for glycolysis (F), glycolytic capacity (G) or glycolytic reserve (H; n=6).
I-L. Neither IFNγ nor IL-4 significantly affected OCR as indicated by the metabolic profile (I) and by analysis of mean values for basal respiration (J), maximal respiration (K) or ATP production (L; n=6).

Figure 1

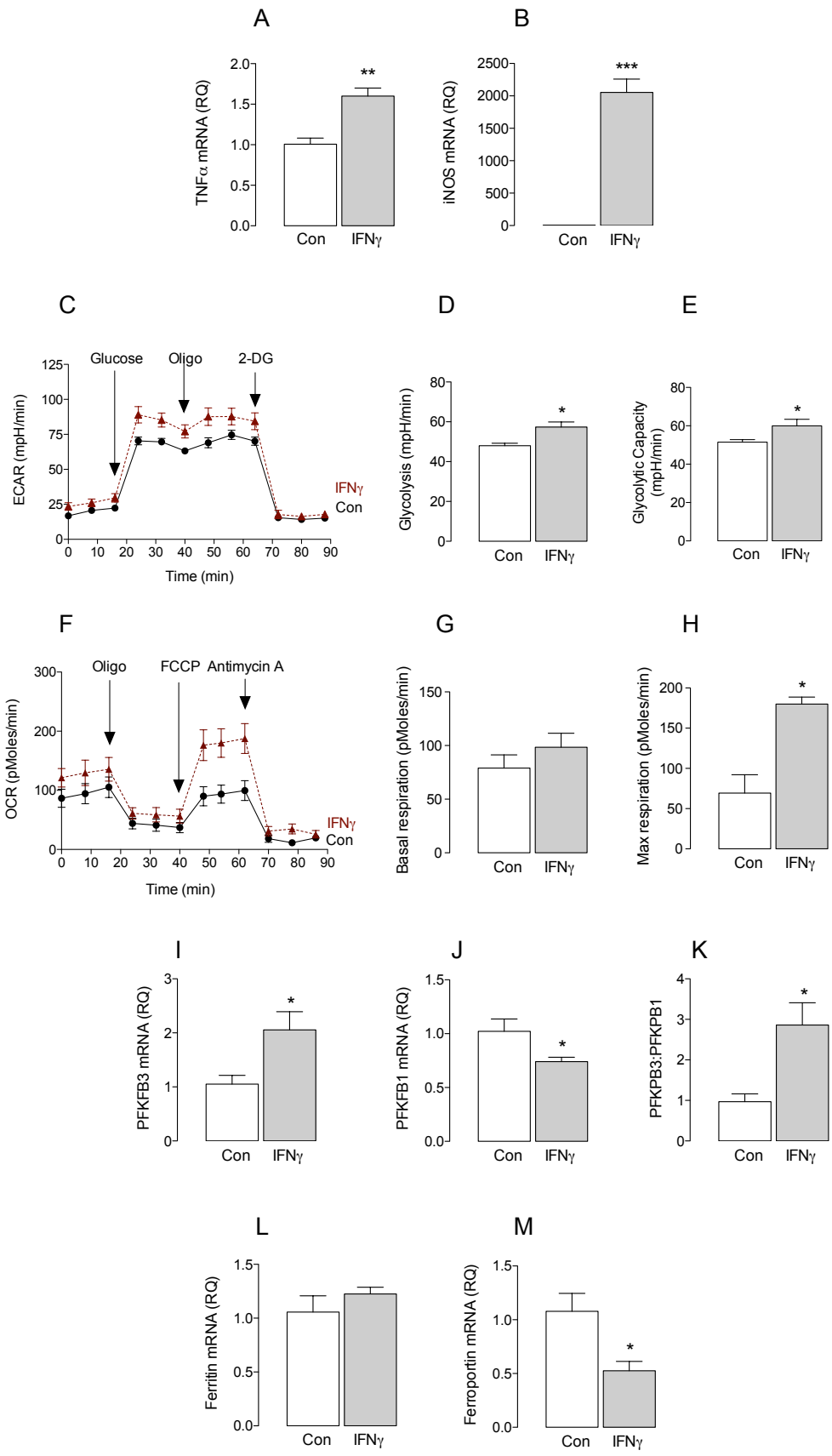
A
TNFα mRNA (RQ)
2.0
1.5
1.0
0.5
0.0
**
Con
IFNγ
B
iNOS mRNA (RQ)
2500
2000
1500
1000
500
0
***
Con
IFNγ
C
Glucose
Oligo
2-DG
ECAR (mpH/min)
125
100
75
50
25
0
0 10 20 30 40 50 60 70 80 90
Time (min)
IFNγ
Con
D
Glycolysis (mpH/min)
80
60
40
20
0
*
Con
IFNγ
E
Glycolytic Capacity (mpH/min)
80
60
40
20
0
*
Con
IFNγ
F
Oligo
FCCP
Antimycin A
OCR (pMoles/min)
300
200
100
0
0 10 20 30 40 50 60 70 80 90
Time (min)
IFNγ
Con
G
Basal respiration (pMoles/min)
150
100
50
0
Con
IFNγ
H
Max respiration (pMoles/min)
200
150
100
50
0
*
Con
IFNγ
I
PFKFB3 mRNA (RQ)
3
2
1
0
*
Con
IFNγ
J
PFKFB1 mRNA (RQ)
1.5
1.0
0.5
0.0
*
Con
IFNγ
K
PFKPB3:PFKPB1
4
3
2
1
0
*
Con
IFNγ
L
Ferritin mRNA (RQ)
1.5
1.0
0.5
0.0
Con
IFNγ
M
Ferroportin mRNA (RQ)
1.5
1.0
0.5
0.0
*
Con
IFNγ

Figure 2

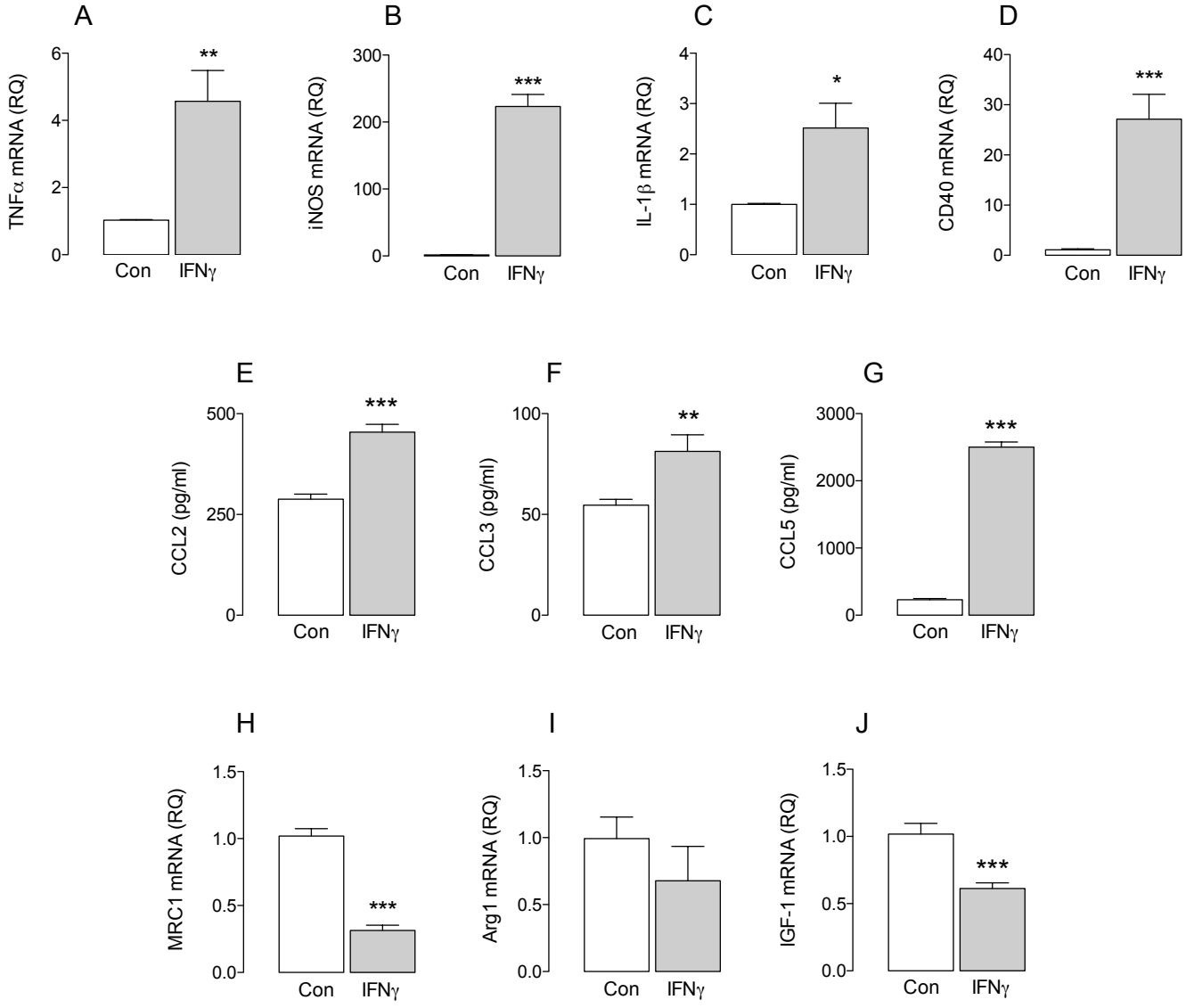
A
TNFα mRNA (RQ)
6
4
2
0
**
Con
IFNγ
B
iNOS mRNA (RQ)
300
200
100
0
***
Con
IFNγ
C
IL-1β mRNA (RQ)
4
3
2
1
0
*
Con
IFNγ
D
CD40 mRNA (RQ)
40
30
20
10
0
***
Con
IFNγ
E
CCL2 (pg/ml)
500
250
0
***
Con
IFNγ
F
CCL3 (pg/ml)
100
50
0
**
Con
IFNγ
G
CCL5 (pg/ml)
3000
2000
1000
0
***
Con
IFNγ
H
MRC1 mRNA (RQ)
1.5
1.0
0.5
0.0
***
Con
IFNγ
I
Arg1 mRNA (RQ)
1.5
1.0
0.5
0.0
Con
IFNγ
J
IGF-1 mRNA (RQ)
1.5
1.0
0.5
0.0
***
Con
IFNγ

Figure 3

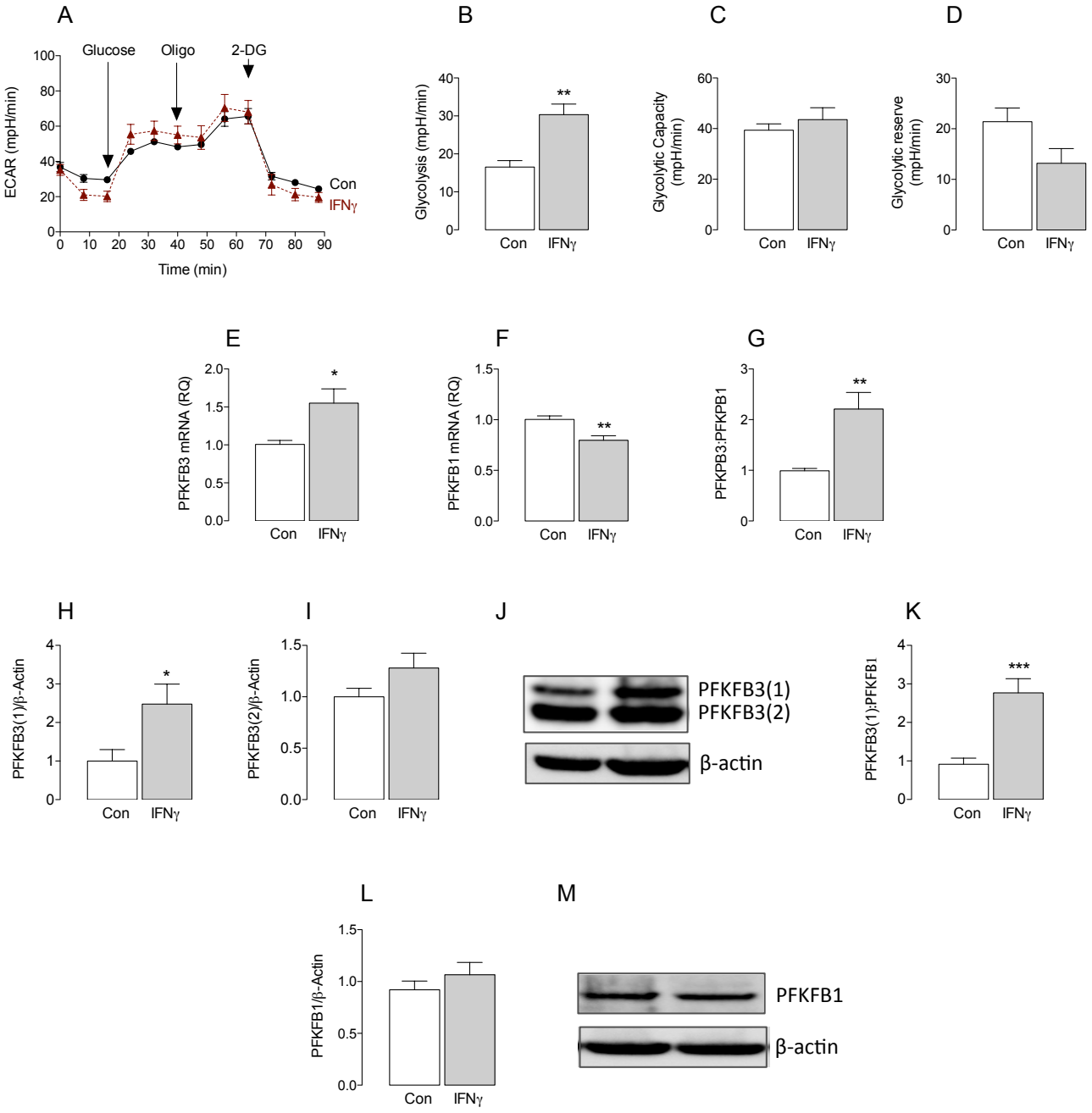
A
Glucose
Oligo
2-DG
ECAR (mpH/min)
Time (min)
Con
IFNγ
B
Glycolysis (mpH/min)
C
Glycolytic Capacity (mpH/min)
D
Glycolytic reserve (mpH/min)
E
PFKFB3 mRNA (RQ)
F
PFKFB1 mRNA (RQ)
G
PFKPB3:PFKPB1
H
PFKFB3(1)/β-Actin
I
PFKFB3(2)/β-Actin
J
PFKFB3(1)
PFKFB3(2)
β-actin
K
PFKFB3(1):PFKFB1
L
PFKFB1/β-Actin
M
PFKFB1
β-actin

Figure 4

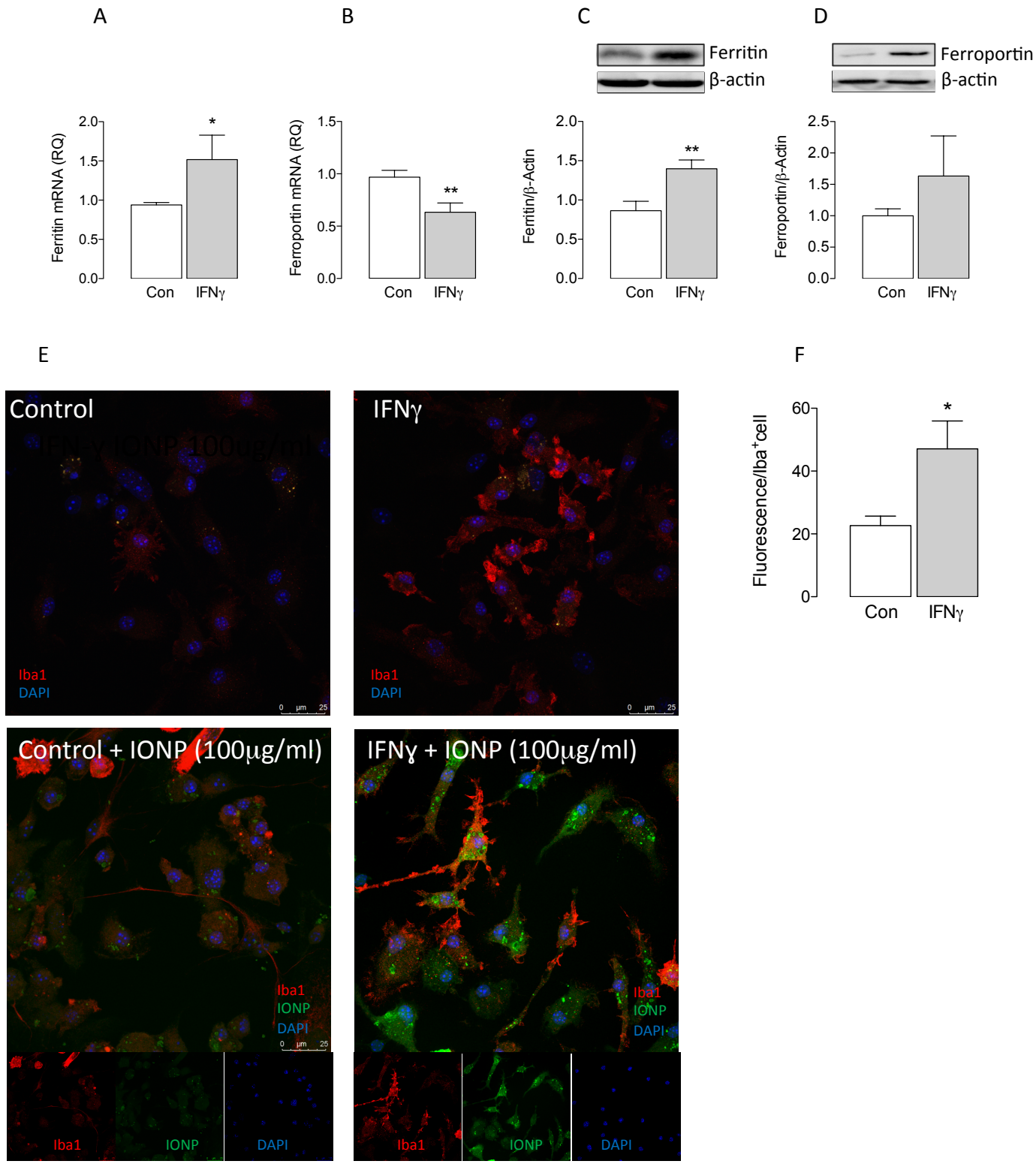
A
B
C
D
Ferritin mRNA (RQ)
Ferroportin mRNA (RQ)
Ferritin/β-Actin
Ferroportin/β-Actin
Con
IFNγ
Ferritin
Ferroportin
β-actin
E
F
Control
IFNγ
Control + IONP (100μg/ml)
IFNγ + IONP (100μg/ml)
Iba1
DAPI
IONP
Fluorescence/Iba+cell

Figure 5

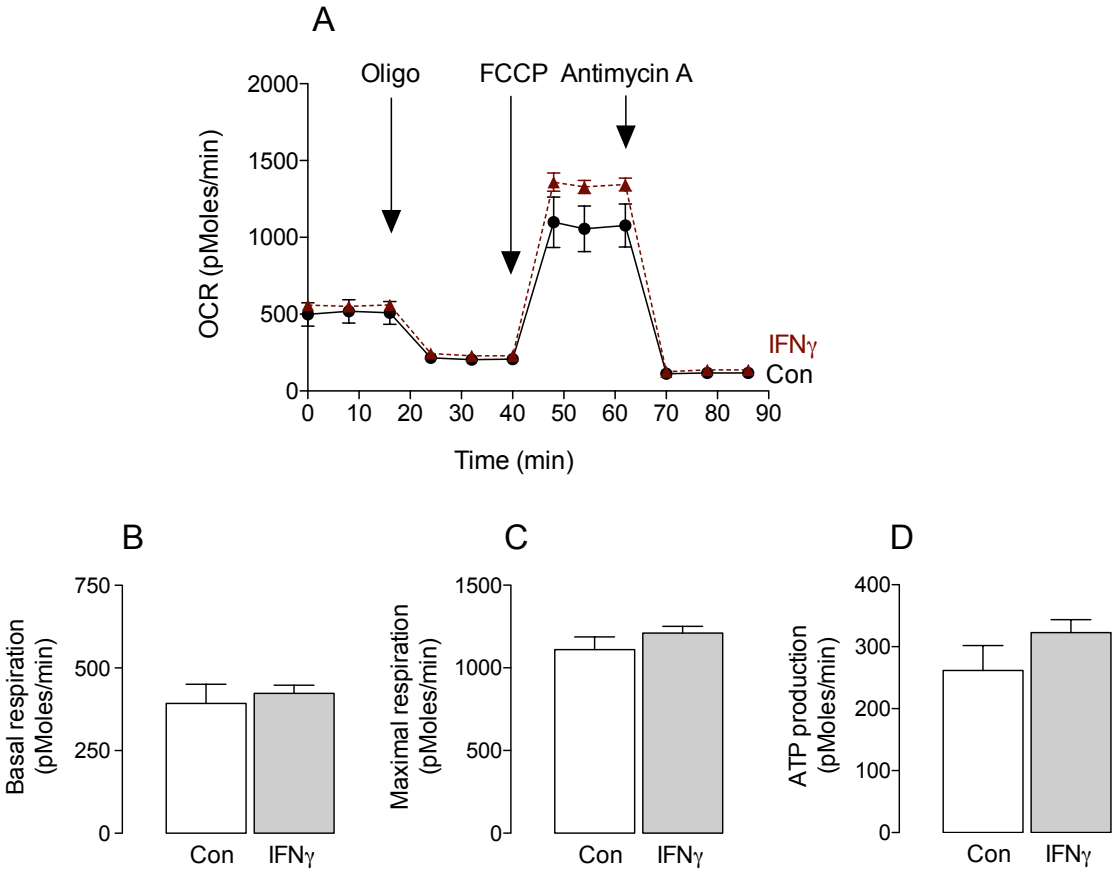
A
Oligo
FCCP
Antimycin A
OCR (pMoles/min)
2000
1500
1000
500
0
0
10
20
30
40
50
60
70
80
90
Time (min)
IFNγ
Con
B
Basal respiration (pMoles/min)
750
500
250
0
Con
IFNγ
C
Maximal respiration (pMoles/min)
1500
1000
500
0
Con
IFNγ
D
ATP production (pMoles/min)
400
300
200
100
0
Con
IFNγ

Figure 6

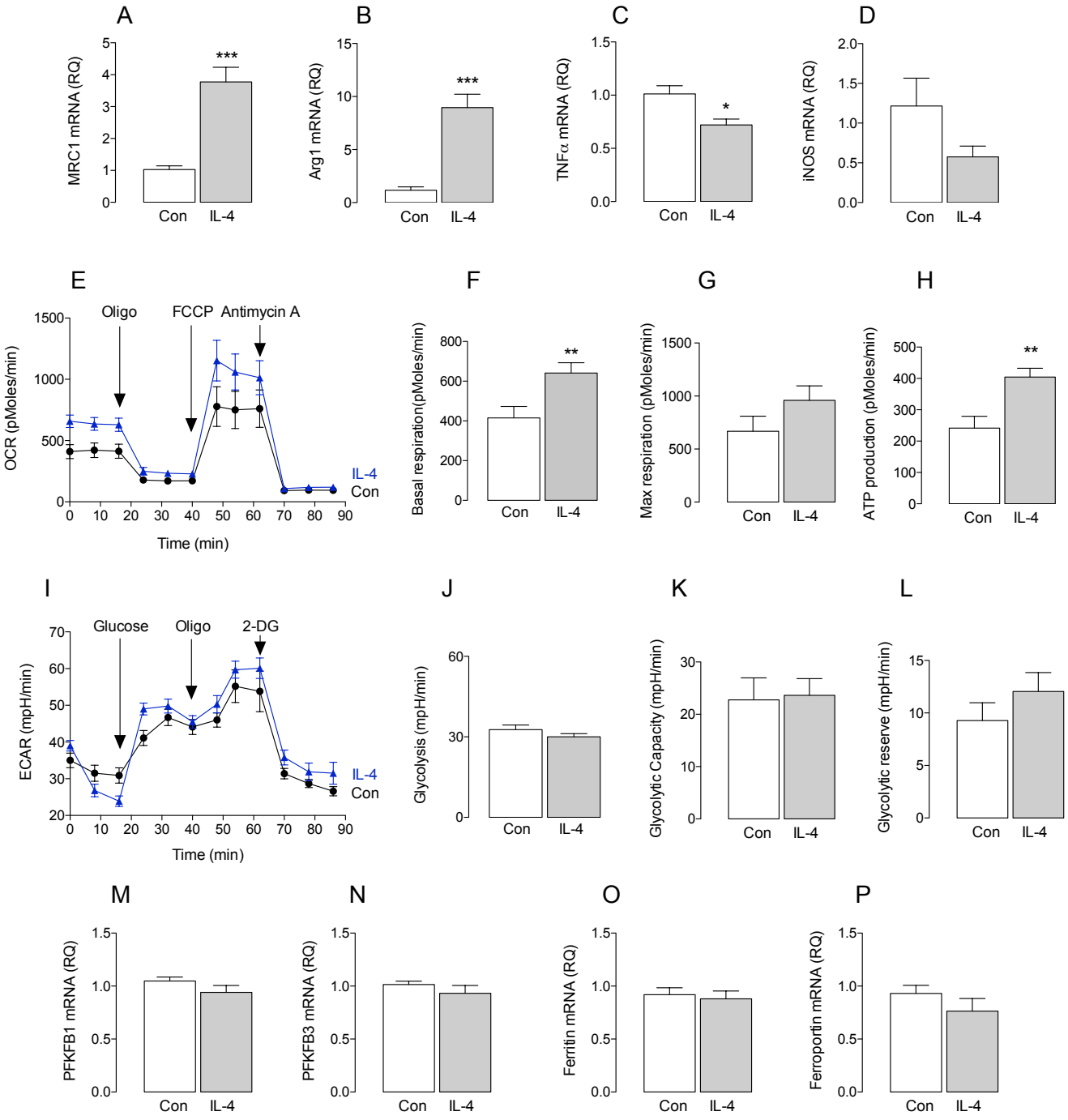
A
MRC1 mRNA (RQ)
***
Con
IL-4
B
Arg1 mRNA (RQ)
***
C
TNFα mRNA (RQ)
*
D
iNOS mRNA (RQ)
E
OCR (pMoles/min)
Oligo
FCCP
Antimycin A
IL-4
Con
Time (min)
F
Basal respiration(pMoles/min)
**
G
Max respiration (pMoles/min)
H
ATP production (pMoles/min)
**
I
ECAR (mpH/min)
Glucose
Oligo
2-DG
IL-4
Con
Time (min)
J
Glycolysis (mpH/min)
K
Glycolytic Capacity (mpH/min)
L
Glycolytic reserve (mpH/min)
M
PFKFB1 mRNA (RQ)
N
PFKFB3 mRNA (RQ)
O
Ferritin mRNA (RQ)
P
Ferroportin mRNA (RQ)

Figure 7

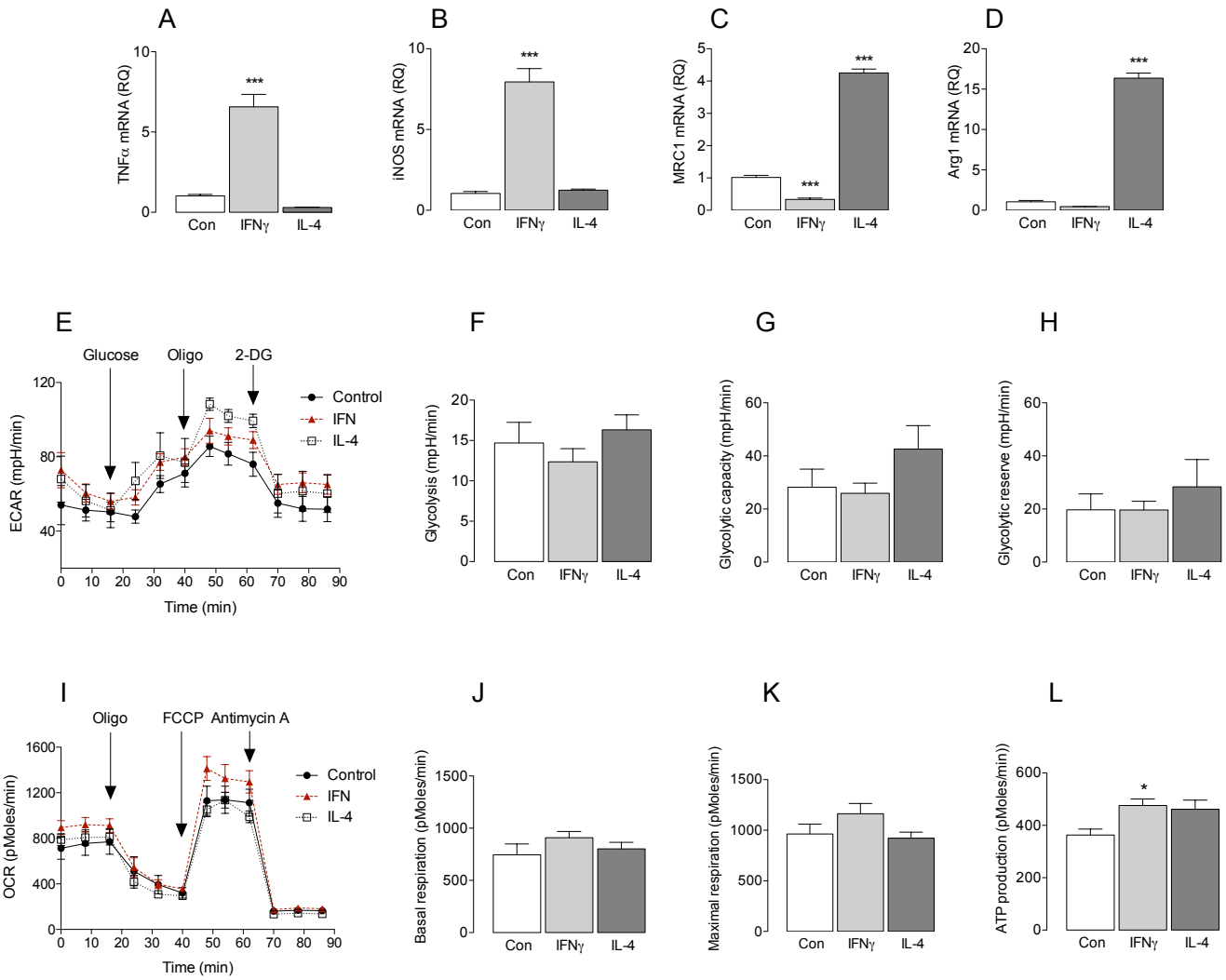
A
TNFα mRNA (RQ)
10
5
0
***
Con
IFNγ
IL-4
B
iNOS mRNA (RQ)
10
5
0
***
Con
IFNγ
IL-4
C
MRC1 mRNA (RQ)
5
4
3
2
1
0
***
***
Con
IFNγ
IL-4
D
Arg1 mRNA (RQ)
20
15
10
5
0
***
Con
IFNγ
IL-4
E
Glucose
Oligo
2-DG
ECAR (mpH/min)
120
80
40
0 10 20 30 40 50 60 70 80 90
Time (min)
Control
IFN
IL-4
F
Glycolysis (mpH/min)
20
15
10
5
0
Con
IFNγ
IL-4
G
Glycolytic capacity (mpH/min)
60
40
20
0
Con
IFNγ
IL-4
H
Glycolytic reserve (mpH/min)
60
40
20
0
Con
IFNγ
IL-4
I
Oligo
FCCP
Antimycin A
OCR (pMoles/min)
1600
1200
800
400
0
0 10 20 30 40 50 60 70 80 90
Time (min)
Control
IFN
IL-4
J
Basal respiration (pMoles/min)
1500
1000
500
0
Con
IFNγ
IL-4
K
Maximal respiration (pMoles/min)
1500
1000
500
0
Con
IFNγ
IL-4
L
ATP production (pMoles/min))
600
400
200
0
*
Con
IFNγ
IL-4